RSC Advances

PAPER

View Article Online
View Journal | View Issue

Cite this: *RSC Adv.*, 2016, **6**, 70174

The impact of MOF feasibility to improve the desalination performance and antifouling properties of FO membranes†

Alireza Zirehpour,[a] Ahmad Rahimpour,*[a] Saeed Khoshhal,[a] Mostafa Dadashi Firouzjaei[b] and Ali Asghar Ghoreyshi[a]

Received 5th June 2016
Accepted 16th July 2016

DOI: 10.1039/c6ra14591d

www.rsc.org/advances

In this study, a hydrophilic metal–organic framework (MOF) was applied to improve the performance of a cellulosic membrane for forward osmosis (FO) desalination application. The characterization results confirmed that the MOF particles existed within the matrix of the modified membrane. The MOF loading led to adjustment of the membranes in terms of overall porosity, pore inter-connectivity and hydrophilicity. These features caused an improvement in the pure water permeability (72%) and reduce the structural parameter of the modified membrane to 136 μm. The FO water flux of the modified membrane enhanced by about 180% compared to an unmodified membrane, without decreasing its selectivity. FO fouling experiments were performed with a feed solution comprising a model organic foulant. The results demonstrated that the modification considerably improved the membrane antifouling properties when compared to the unmodified membranes. Water flux was also more easily recovered through physical cleaning for the modified membrane. The modified membrane was continuously tested under FO seawater desalination to investigate the performance stability. The modified membrane demonstrated a noteworthy water flux of above 30 LMH, using a 2 M NaCl draw solution. The modified membrane developed in this study exhibited outstanding permselectivity compared to ones reported in the literature.

1. Introduction

Seawater desalination has been the focus of many research studies to overcome the fresh water scarcity challenges in most countries.[1] Forward osmosis (FO) has been advertised as a high-recovery and low-energy water filtration as well as desalination technique that shows great promise in addressing the general water crisis.[2–5] In addition, FO is among the most effective strategies to achieve high removal of contaminants from water.[6] FO works based on a dense hydrophilic semipermeable membrane that separates two solutions called the feed solution (FS) and draw solution (DS), and an osmotic pressure gradient which is the driving force of the process.[7] Because of the absence of external hydraulic pressure, FO has several unique advantages in terms of low energy consumption, efficient water recovery, low membrane fouling, and easy fouling removal, compared to conventional pressure-driven desalination processes such as reverse osmosis (RO).[8,9] However, the lack of effective membranes and suitable DS had hindered the FO process development.[10,11] In this regard, various researches focused on FO membranes development during last decade. Different kinds of FO membranes including phase-inversion, thin-film composite (TFC) and layer-by-layer (LbL) have been fabricated.[12–22] Commonly, a high performance FO membrane requires (1) a thin selective layer with high water permeability as well as low solute permeability, (2) a highly porous and hydrophilic scaffold layer with proper water transport as well as low internal concentration polarization (ICP) and (3) worthy anti-fouling and anti-biofouling properties.[23–25]

The ICP is one of the most important FO process challenges causing to reduce the FO performance.[26–28] ICP is mainly influenced by specific characteristics of membrane sub layer, such as the porosity (ε), tortuosity (τ) and thickness.[29,30] The structural parameter (S, thickness × tortuosity/porosity) has been introduced as an indicative value to quantify the structure contribution of the FO membrane on ICP. Several methods have been carried out to alleviate ICP *via* reducing the membrane thickness[8] and increasing the porosity of sub layer.[31–33] The incorporation of the inorganic fillers as nonporous materials in FO membranes can result in significant changes in the membrane properties such as morphology, hydrophilicity, performance and FO performance.[24,34–37] In this study, metal

[a]*Membrane Research Laboratory, School of Chemical Engineering, Babol University of Technology, Babol, Iran. E-mail: ahmadrahimpour@nit.ac.ir; ahmadrahimpour@yahoo.com; Fax: +98 11 32334204; Tel: +98 11 32334204*

[b]*Department of Material Science and Engineering, Sharif University of Technology, Tehran, Iran*

† Electronic supplementary information (ESI) available. See DOI: 10.1039/c6ra14591d

organic framework (MOF), as a porous nanostructure material, was applied to improve the structure and performance of FO membranes. MOFs as hybrid inorganic–organic compounds are new categories of porous materials with exceptionally large surface area as well as high pore volume. MOFs have better affinity for the polymeric chains than inorganic fillers because of the organic linkers present in their structure. Hence, it is easier to control MOF–polymer interface interactions, and avoid non-selective voids between the phases. The blend of MOF with a polymer to form a composite membrane for gas separation applications has been widely studied.[38] Moreover, liquid separation studies of MOF mixed matrix membranes have been carried out for pervaporation[39,40] and nanofiltration.[41,42]

The current study aims to investigate the impact of incorporating MOF nanomaterial within the cellulose acetate/triacetate (CTA) matrix for improving the FO membrane perm/selectivity, and controlling ICP. Cellulose esters are used in fabrication of FO membranes due to their intrinsic advantages involving low cost, wide availability, high hydrophilicity, low fouling as well as superior chlorine resistance.[43,44] Copper-based MOF (Cu-BTC, btc = benzene-1,3,5-tricarboxylate) is considered as one of the most hydrophilic MOFs with a good affinity and structural stability toward water.[45,46] Hence, this kind of MOF was chosen to improve the FO membranes. To the best knowledge of the authors, this is the first study addressing Cu-BTC as a modifier to improve the CTA membrane in terms of structural properties and FO performance during seawater desalination.

2. Materials and methods

2.1. Chemicals and reagents

CA (39.8 wt% acetyl and average $M_n \sim 30\,000$) CTA (43–49 wt% acetyl) were provided from Eastman (USA). 1,4-Dioxane (≥99.5% purity), acetone (≥99% purity), maleic acid (≥99% purity), methanol (≥99.8% purity), lactic acid and sodium alginate were obtained from Sigma-Aldrich (MO, USA). Sodium chloride (NaCl, 99% purity) was also purchased from Merck-Millipore (Germany). MOF applied, Cu-BTC, was synthesized based on our previous study, where we investigated and optimized the MOF structure by considering the temperature and solvent content effects on crystallinity, textural properties and hydrogen storage capacity.[47] Characterizations of the synthesized MOF were presented in the ESI, Table S1 and Fig. S1–S3.†

2.2. Membranes preparation

Asymmetric FO mixed matrix membranes were prepared by phase inversion *via* immersion precipitation method. Blank CTA membrane was prepared by mixing CA/CTA (16.7 wt%, 4 : 1 ratio), methanol (5 wt%) and lactic acid (5.7 wt%) in dioxane/acetone (3 : 1 ratio) as solvent. For preparation of mixed matrix membranes, two different MOF contents, 3 wt% and 6 wt% (based on polymer content) were loaded in the casting solution. The specifications of casting solution are given in Table 1. MOFs were dispersed in solvents and then subjected to the ultrasonic bath for 60 min, prior to dissolution of CTA and CA in the blend solution. Then, the casting solution kept under continuous stirring until the solution became completely homogenous. Afterward the solution was kept steady to remove the bubbles. The solution was sprinkled and casted on a flat glass plate using homemade casting knife with 75 micron thickness, followed by 30 s partial solvents evaporation. The cast film was immersed in a coagulation bath containing deionized (DI) water with temperature of 4 °C. The prepared membranes were kept in DI water at room temperature. Finally, the membranes were annealed at 80 °C for 15 min in water and stored in DI water prior to being used. The membranes were denoted as Blank, MO-1 and MO-2, containing 0, 3 and 6 wt% of MOF, respectively.

2.3. Membrane characterization

The morphological studies were accomplished by field emission scanning electron microscopy (FESEM) and atomic force microscopy (AFM). The cross section and top surface morphologies of the membranes (Blank, MO-1 and MO-2) were characterized by FESEM (MIRA3 TESCAN) equipped with an energy-dispersive X-ray (EDX) spectroscopy. All samples were dried at room temperature in vacuum for 24 h, and then coated with a uniform gold layer before observation. The AFM device was a Nanosurf scanning probe-optical microscope (EasyScan II, Swiss). The surface roughness parameters of the membranes which are expressed in terms of the mean roughness (Sa), was calculated from AFM images using tapping mode method *via* Nanosurf Easy Scan software in a scan area of 5 μm × 5 μm.

In order to study the membranes hydrophilicity, the surface water contact angle of the membranes was measured using a contact angle measuring instrument [G10, KRUSS, Germany]. To minimize the experimental error, the contact angle was measured at five random locations of each sample and the average value was reported.

Dope solution viscosities with different concentration of MOFs were measured using a Brookfield (DV2T) viscometer at 25 °C (varied rotational speed of the LV spindle).

Overall porosity (ε) of the membranes was obtained by gravimetric measurement using the following equation:[48,49]

$$\varepsilon = \frac{(m_{wet} - m_{dry})/\rho_w}{(m_{wet} - m_{dry})/\rho_w + (m_{dry}/\rho_p)} \times 100 \quad (1)$$

where m_{dry} and m_{wet} are dry and wet mass of membrane respectively, ρ_w is the water density and ρ_p is the polymer density.

Table 1 Composition and viscosity of the casting solutions

Membrane	Polymer *vs.* filler (wt%)		Viscosity at shear rate of 10 s^{-1} (Pa s)
	CA/CTA (ratio 4 : 1)	MOF	
Blank	100	0	33.5
MO-1	97	3	37.6
MO-2	94	6	46.3

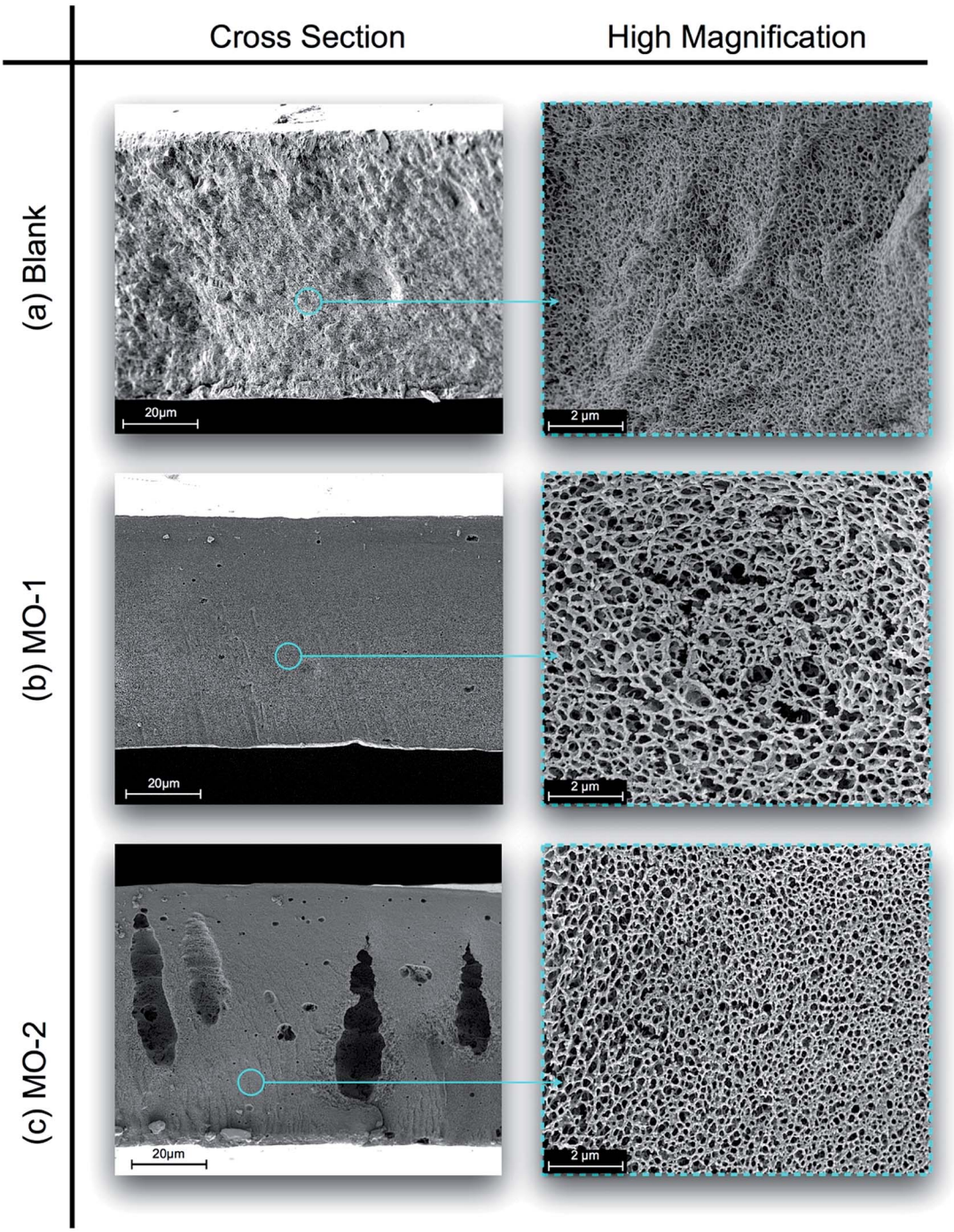

Fig. 1 Cross section FE-SEM images of FO membranes, (a) blank, (b) MO-1, (c) MO-2.

2.4. FO performance and transport properties evaluation of the membranes

The FO performance of the membranes (water flux and salt flux) was determined in a laboratory-scale FO setup. The unit includes two channels with dimensions of 80 mm length, 37 mm width and 5 mm depth, giving the same effective membrane area of 30 cm^2 in both sides. Two diaphragm pumps (Headon, 2.2 LPM) were applied to pump the solutions. Two adjustable flow meter were used to set crossflow velocity of 21 cm s^{-1} in both the FS and DS channels. Both the pressure and temperature of the feed and draw streams were monitored and fixed. Concentrated NaCl solutions (0.5, 1, 1.5 and 2 M) were used as DS. DI water was used as FS.

The FO water flux J_w was obtained by measuring the weight change of FS by a computer at 1 min intervals, using following equation:

$$J_w = \frac{\Delta V_{feed}}{A_m \times \Delta t} \quad (2)$$

where ΔV_{feed} is the volume changes of FS, A_m is the membrane active surface area and Δt is the evaluating time interval.

The FO salt flux J_s was determined by calculating the change of salt content in the FS based on conductivity measurements using a computer at 10 min intervals:

$$J_s = \frac{V_t C_t - V_0 C_0}{A_m \times \Delta t} \quad (3)$$

where V_t and V_0 are the final and initial volumes of FS, respectively; C_t and C_0 are the final and initial salt concentrations of FS, respectively.

The intrinsic membrane active layer characteristics, water permeability coefficient (A) and solute permeability coefficient (B), as well as S parameter of the membranes were characterized based on methodology developed by Tiraferri *et al.*[50] The methodology includes a single FO experiment divided into four stages, each utilizing a different DS concentration. The FO water flux and reverse salt flux are measured in each experimental stage and then least-squares non-linear regression fits the eight measured data to the corresponding FO transport equations by using A, B, and S as regression parameters.[50] In order to increase the accuracy of the presented data, an average of three repeated experiments was reported.

2.5. FO fouling experiments

FO fouling experiments were conducted with the MO-1 and blank membranes by the laboratory scale FO setup described in Section 2.4, based on the method described in literature.[51,52] The FS contained of sodium alginate dissolved in water at a concentration of 250 mg L^{-1}. The fouling experiments were performed under active layer facing feed solution (ALFS) mode without spacers and cross flow velocities of 8.5 cm s^{-1} in both the FS and DS channels. After loading a fresh membrane into FO cell, a baseline experiment was performed using a foulant-free FS (DI water) to measure the amount of flux declines derived exclusively from reverse draw solute diffusion and DS dilution. Sodium chloride DSs were used to generate initial FO water fluxes, J_{w0}, of about 20 L m^{-2} h^{-1} through each of the membranes. This means the membranes were tested under same initial water flux (20 L m^{-2} h^{-1}) but different DS concentration. The fouling experiment was conducted (with alginate in the FS) at the same initial flux as the baseline experiment. Then, fouling experiment data were corrected to eliminate the flux decline from reverse draw solute diffusion and DS dilution.[51,53] Hence the presented data reflect only the flux decline because of membrane fouling. The baseline and fouling experiments were conducted up to 24 hours. In order to evaluate the extent of irreversible fouling, the membranes were washed for 15 min using 15 mM NaCl solution through the feed and draw compartments at a cross-flow velocity of 21 cm s^{-1}. Ultimately, the FO water flux through the washed membrane was measured under the same conditions as the baseline experiment.

Table 2 Contact angle and overall porosity of the fabricated membranes, all data reported as average of three repeated measurements

Membrane	Contact angle (deg.)	Overall porosity (%)
Blank	67.3 ± 1.5	69.5 ± 0.5
MO-1	55.2 ± 1.2	89.1 ± 0.5
MO-2	51.3 ± 1.7	78.2 ± 0.5

3. Results and discussions

3.1. Membrane structure and morphology

Fig. 1 shows the cross sections FE-SEM images of the blank and MOFs modified membranes at different magnifications. The images indicated typical asymmetric structure for membranes, consisting of two regions: (1) a thin skin layer region at the upstream side of the membrane, (2) a thick porous support layer on the downstream side of the membrane.

As shown in the high magnification SEM images, all membranes had a fully sponge-like structure with interconnecting pores. The membranes containing MOF exhibited more porous cross-section morphology and pore interconnectivity than those of the blank membrane. As a result,

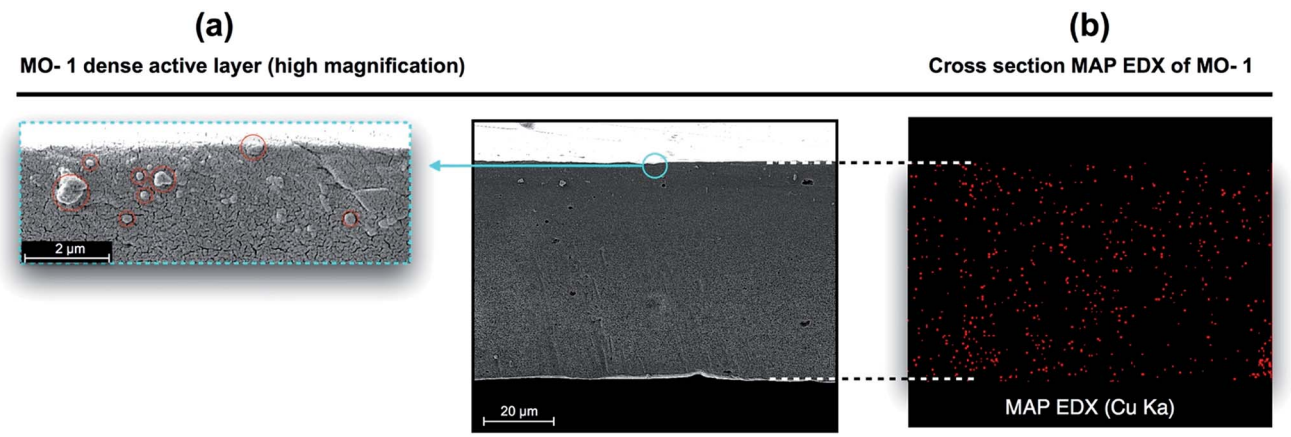

Fig. 2 (a) High magnification FESEM images of the MO-1 membrane active layer, (b) cross section MAP EDX analysis of the MO-1 membrane for copper.

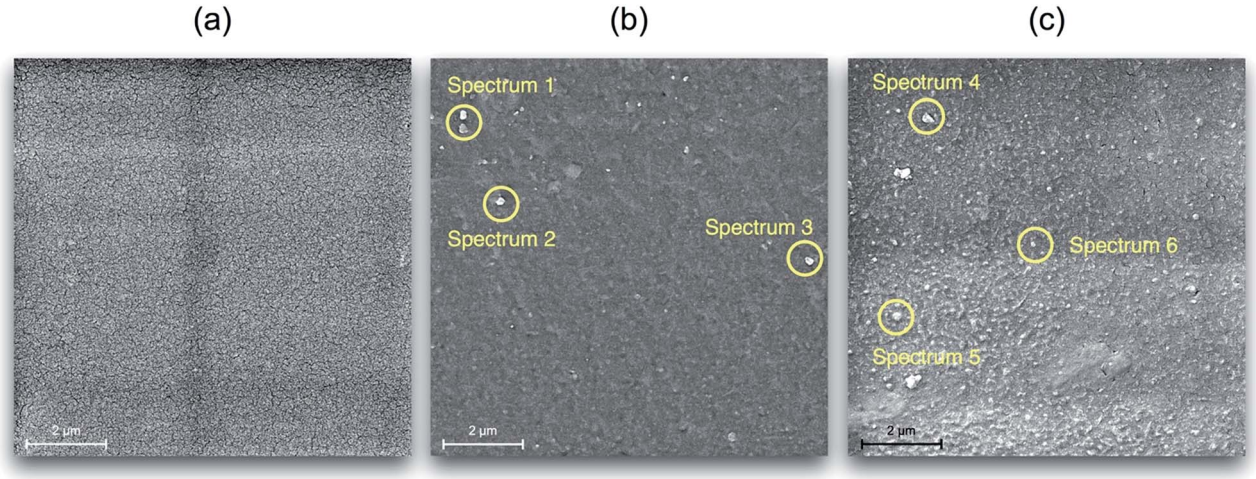

EDX Spectra (MO-1)

Spectrum	Cu wt.%
1	2.1
2	0.9
3	1.6

(d)

EDX Spectra (MO-2)

Spectrum	Cu wt.%
4	2.8
5	1.9
6	0.6

(e)

Fig. 3 Top surface FE-SEM images of the fabricated membranes, (a) blank (b) MO-1, (c) MO-2, (d) EDX results of different spectrums of MO-1 surface, (e) EDX results of different spectrums of MO-2 surface.

a high porosity of about 89% was obtained for MO-1 membrane containing 3 wt% MOF (Table 2). Nevertheless, the higher MOF loading resulted in a less porous structure, as obtained for MO-2 membrane. Generally, a membrane with high porosity is more favoured in FO process.

The differences between the membrane structures are generally due to MOF loading in the casting solution and hence change affecting the thermodynamic and kinetic of the phase inversion process. High-porosity membrane is the result of situations that the kinetic or the thermodynamic effects accelerate the exchange rate of phase inversion. In this situation, the microstructural development confirmed that the appropriate amount of MOF helped to increase the thermodynamic instability as well as the exchange rate of solvent-non solvent and consequently, a more porous structure formed in the MO-1 membrane. However, less porous structure observed in the MO-2 membrane can be attributed to the kinetic hindrance due to a greater viscosity of the casting solution, which overwhelms the thermodynamic factor (Table 1).[54–58]

Fig. 2 shows MAP EDX analysis and high magnification image of the MO-1 membrane top layer. The image indicates many sub-microns MOF particles existing within the MO-1 selective layer (Fig. 2a). The CTA matrix seems to surround completely MOF particles, and no gaps observed around them. Additionally, the MAP EDX analysis well recognized the cupper within the membrane matrix. This proved that the Cu–BTC/MOF particles were successfully embedded in polymer matrix, and a homogeneous distribution was achieved (Fig. 2b).

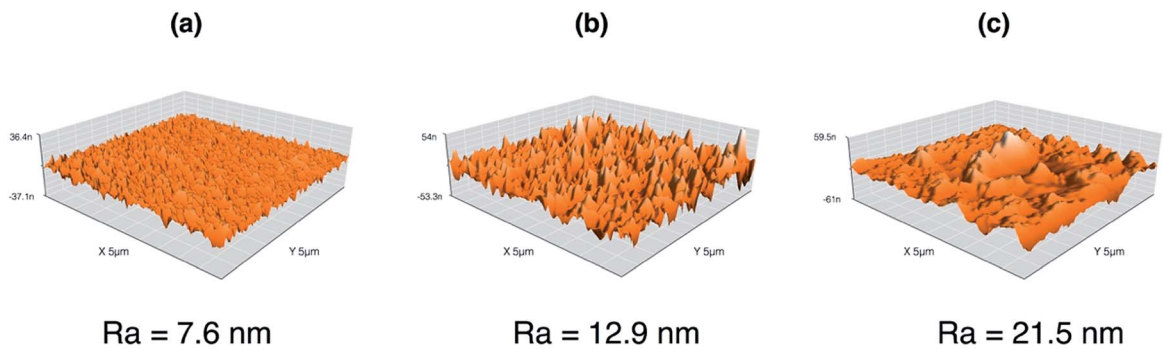

Fig. 4 Three-dimensional surface AFM images of the membranes, (a) blank, (b) MO-1, (c) MO-2.

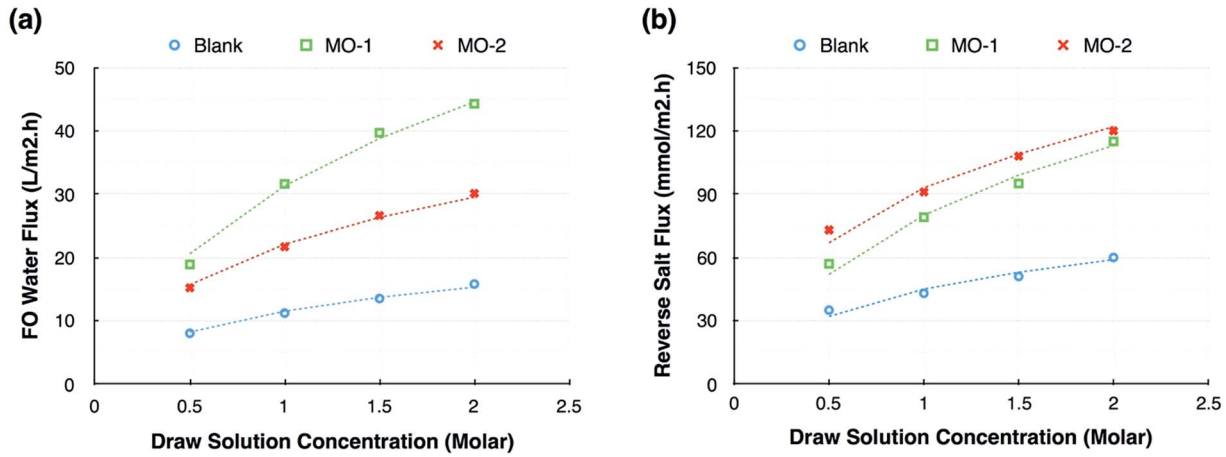

Fig. 5 Experimental (points) and predicted (dash lines) data of (a) FO water flux and (b) reverse salt flux for the fabricated membranes using different concentrations of NaCl DSs, (T = 25 °C, feed = DI water, orientation = ALFS). The predicted data were calculated by the intrinsic membrane active layer and support layer characteristics (A, B and S parameter).

Fig. 3 illustrates the top surface FESEM micrograph of the membranes. The images show that the membrane surfaces are relatively dense and smooth. All the membranes show similar morphology with no visual pores observed at the taken magnification. MOF particles can be easily seen in the surface of MOF mixed matrix membrane (bright points in Fig. 3b and c). The EDX spectra of six spots on the membranes surface were carried out to verify the MOF particles (Fig. 3d and e).

The results confirmed that the MOF particles existed within the active layer of the modified membranes and on their surface as well. The presence of MOF particles on the surface of modified membranes occurred during membrane formation, in which the high affinity of MOF particles to water causes the particles to migrate to the membrane top layer and concentrate at the water/membrane boundary to minimize the interfacial energy.[59–61] However, lots of agglomerated particles on the active layer of MO-2 membrane may reduce selective layer integrity and thus decrease its performance.

As shown in AFM images, the rougher surface was introduced for mixed matrix membranes containing MOF (Fig. 4). The surface roughness of the MO-1 and MO-2 membranes increased about two and three times, respectively which may

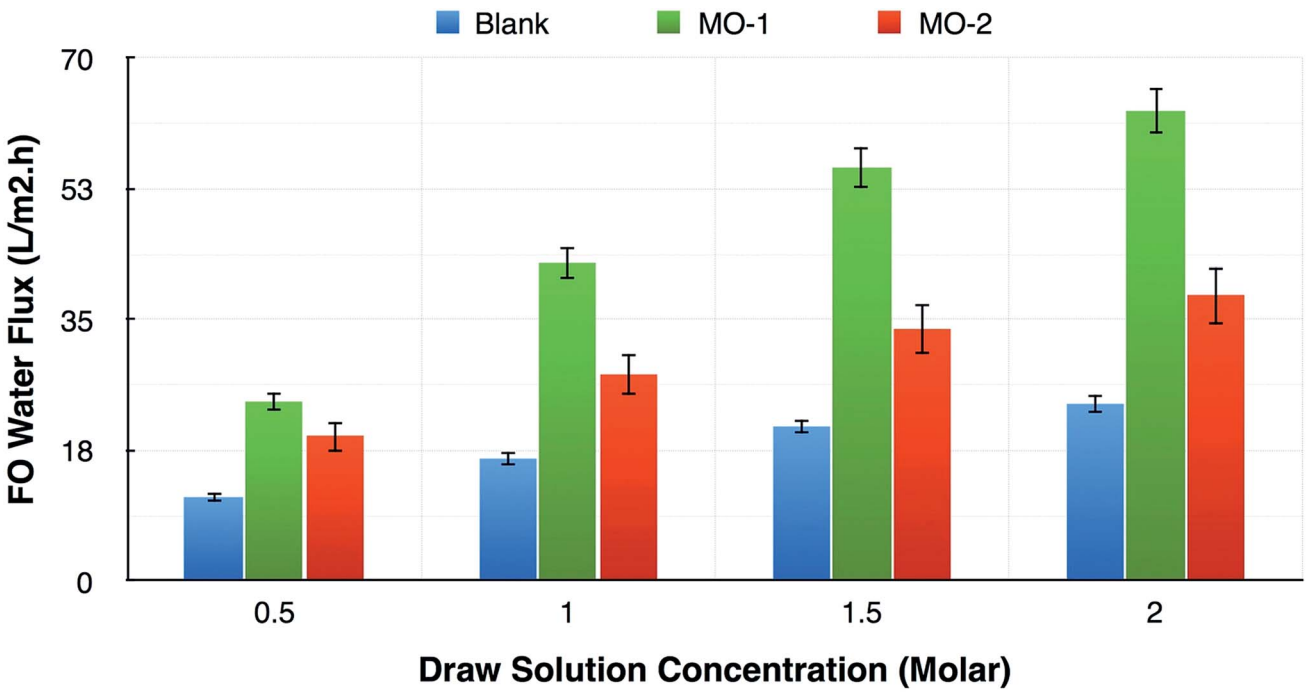

Fig. 6 FO water flux of the membranes in ALDS mode and using different DS concentrations (T = 25 °C, feed = DI water), error bars represent standard deviation over runs.

Table 3 Summery of the transport parameters *A*, *B* and the *S* values of the membranes. The data were calculated by the algorithm developed by Tiraferri *et al.*[50] The related coefficients of determination (R^2) and the corresponding CV are obtained from the same method

Membrane	*A* (L m^{-2} h^{-1} bar^{-1})	*B* (L m^{-2} h^{-1})	*B*/*A* (bar^{-1})	*S* (μm)	Thickness (μm)	τ/ε	R^2 (J_v)	R^2 (J_s)	CV (%)
Blank	0.82	0.157	0.191	579	75 ± 5	7.7	0.987	0.951	6.8
MO-1	1.41	0.178	0.126	136	67 ± 8	2	0.988	0.979	9.7
MO-2	1.73	0.354	0.203	318	70 ± 5	4.5	0.985	0.964	8.1

be attributed to the presence of MOF particles on their surfaces.

The quality of the interface in the membranes, that is, the static adhesion strength as well as the interfacial interaction, usually plays a very important role in the FO membranes to transfer the water. In this regard, the contact angle analysis was used to evaluate the surface hydrophilicity or wettability of the FO membranes. As revealed in Table 2, the contact angle of the MO-2 membrane decreased about 24%, compared to the blank membrane, indicating the membrane wettability was improved. It can be attributed to presence of the hydrophilic MOF particles within the membrane surface.

The results obviously indicated that MOF loading led to adjustment of the modified membranes in terms of porosity and pore inter-connectivity. In addition, hydrophilic surface and highly porous structure of MOF may selectively absorb water and provide alternative transport pathways for water media through the membrane. These features have been tailored to improve the FO performance of the resultant membranes.

3.2. Membrane performance

In order to investigate the effects of MOF on the membrane performance, FO water flux (J_w) and solute flux (J_s) of the fabricated membranes were evaluated. High water flux and low reverse solute leakage are essential for a high-quality FO membrane. The osmotic water flux (Fig. 5a) and reverse salt flux (Fig. 5b) of the membranes were measured as a function of DS concentration when DI water was used as FS.

Both the experimental data and the predicted data from the method developed by Tiraferri *et al.* have been presented.[50]

Increasing the DS concentration leads to a higher water flux because of a greater osmotic driving force across the membranes.[62] The reverse solute leakage from DS to FS was increased due to a higher salt concentration gradient through the membrane. As it can be seen from Fig. 5a, MOF loading caused a much higher water flux in the modified membranes compared to the blank membrane. For example, MOF loading exhibited about 180% higher FO water flux in the MO-1 membrane than that of the unmodified membrane (2 M NaCl solution as DS). Higher amount of MOF (6 wt%) decreased the FO water flux. On the other hand, the incorporating of MOF in the membrane matrix resulted in a slight increase in solute flux of the modified membranes compared to the blank membrane.

Fig. 6 shows the membranes performance at active layer facing DS (ALDS) mode. The FO water flux of the membranes was considerably increased in ALDS mode. Generally, the water flux obtained from the ALDS mode is greater than that in the ALFS mode due to the lower ICP phenomenon in the ALDS mode.[63,64] Similar to the observed trend in Fig. 5a, the MO-1 membrane exhibited the highest FO water flux compared to the other membranes in ALDS orientation. The FO water flux reached to about 63 L m^{-2} h^{-1} (2 M NaCl solution as DS).

In order to discuss the experimental trends of FO performance, the intrinsic water (*A*) and solute (*B*) permeability coefficients, the *S* parameter for the membranes were calculated from the FO experimental data, and the results are summarized in Table 3. Moreover, the ratio of tortuosity (τ) to porosity (ε), an

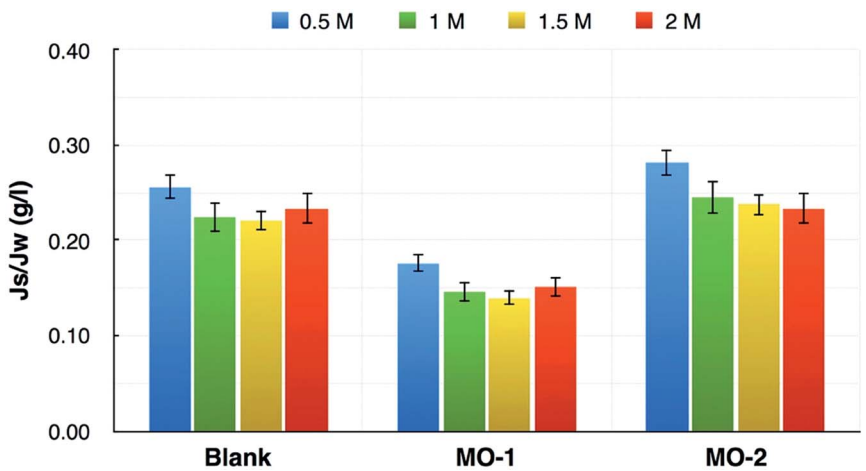

Fig. 7 Specific salt flux of the membranes at different DS concentrations, error bars represent standard deviation over runs.

important ratio directly affects the S parameter, is presented. It is worth mentioning all the R^2 and coefficient of variation (CV) values are within the recommended values of the used methodology. The CVs were calculated between the J_s/J_w ratios of the different stages in each experiment for each the membrane. The results clearly indicate that the membrane properties depend on the amount of MOF loaded. The small amount of MOF particles in the MO-1 membrane led to enhance the water permeability, whereas the addition of more MOF in the MO-2 membrane resulted in higher water permeability of membrane but at the expense of selectivity. The B value amount of the MO-2 was almost twice compared to the MO-1.

Presence of MOF particles may interrupts the CTA chain and causes an increase in polymer free volume.[65] As a result, the water permeability of the membrane is improved. However, high loading of MOF in the MO-2 membrane can cause a lower degree of active layer integrity, reducing membrane efficiency in salt rejection and increasing solute flux.

Despite the fact that MOF loading slightly increased the B value, the B/A ratio as an important FO membrane selectivity parameter reduced in the MO-1 (Table 3). A lower B/A ratio is generally preferred to enhance selectivity, reduce fouling tendency as well as more stable FO processes operation.[62,66,67] As can be seen the B/A ratio of the MO-1 membrane was 0.126 bar^{-1} which is almost 34% smaller than that of the blank membrane (0.191 bar^{-1}). This indicates that MOF loading improved the MO-1 membrane selectivity.

The results implied that the A values were not fully consistent with the FO water flux. This indicated that the hydraulic resistance did not only reflect the FO membrane transport properties.[24] The S parameter, an important FO membrane property which directly affects the ICP, can complete the explanation trends of FO water flux. As shown in Table 3, loading of MOF considerably reduced the S parameter of the modified membranes. For instance, the MO-1 exhibited a much smaller S value (136 μm) compared to the blank membrane (579 μm). This indicates the significant improvement of the mass transfer efficiency for the modified membrane. This is linked to its lower ratio of tortuosity to porosity (τ/ε), as shown in Table 3. However, the S parameter increased to about 318 μm when the MOF loading increased.

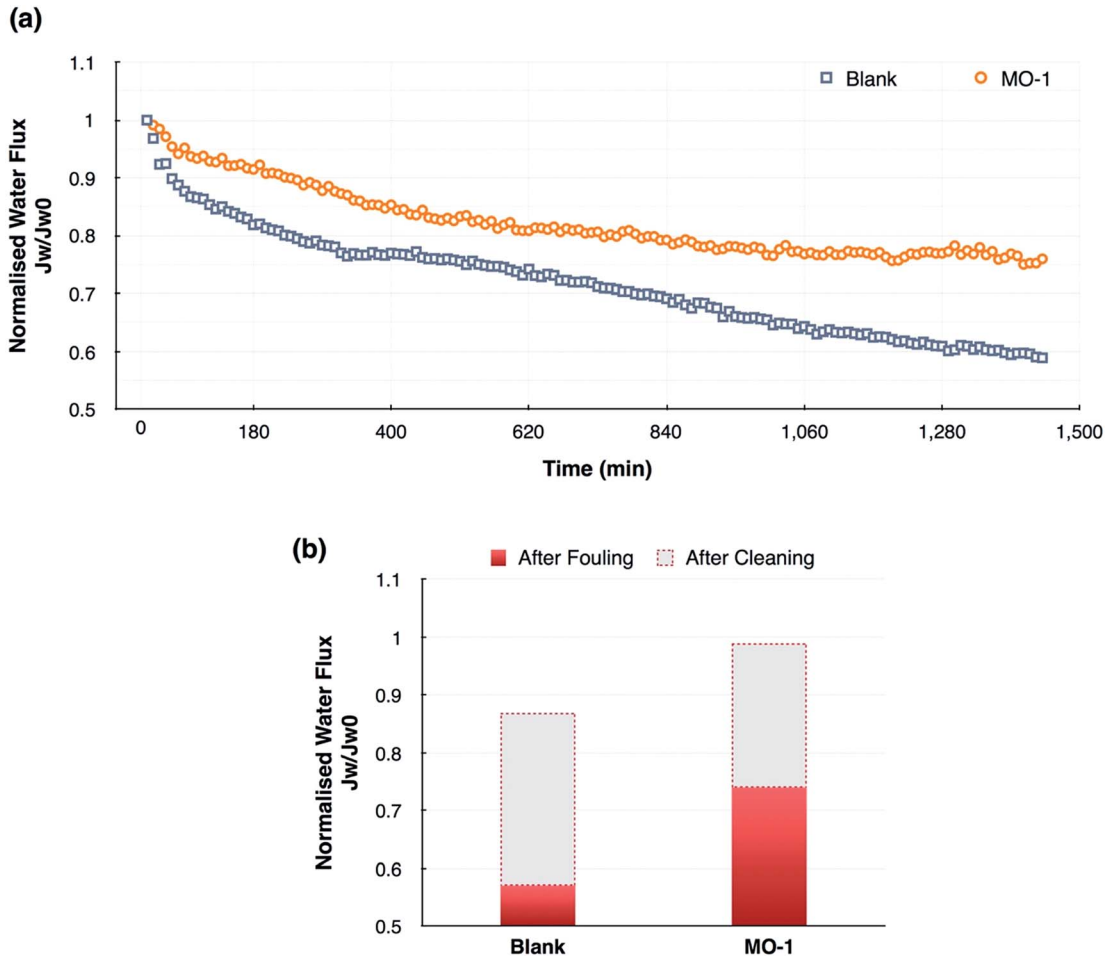

Fig. 8 (a) FO fouling curves for the blank membrane and the modified membranes (MO-1). The FS supplemented with 250 mg L^{-1} of alginate as model organic foulant. The initial permeate water flux of around 20 L m^{-2} h^{-1}. The cross flow velocities of the FS and DS were 8.5 cm s^{-1} ($T = 25$ °C, DS = NaCl 0.5–2 M), (b) comparison between the FO water flux of foaled membrane and recovered after the physical cleaning step. Cross flow velocity during cleaning step was 21 cm s^{-1}.

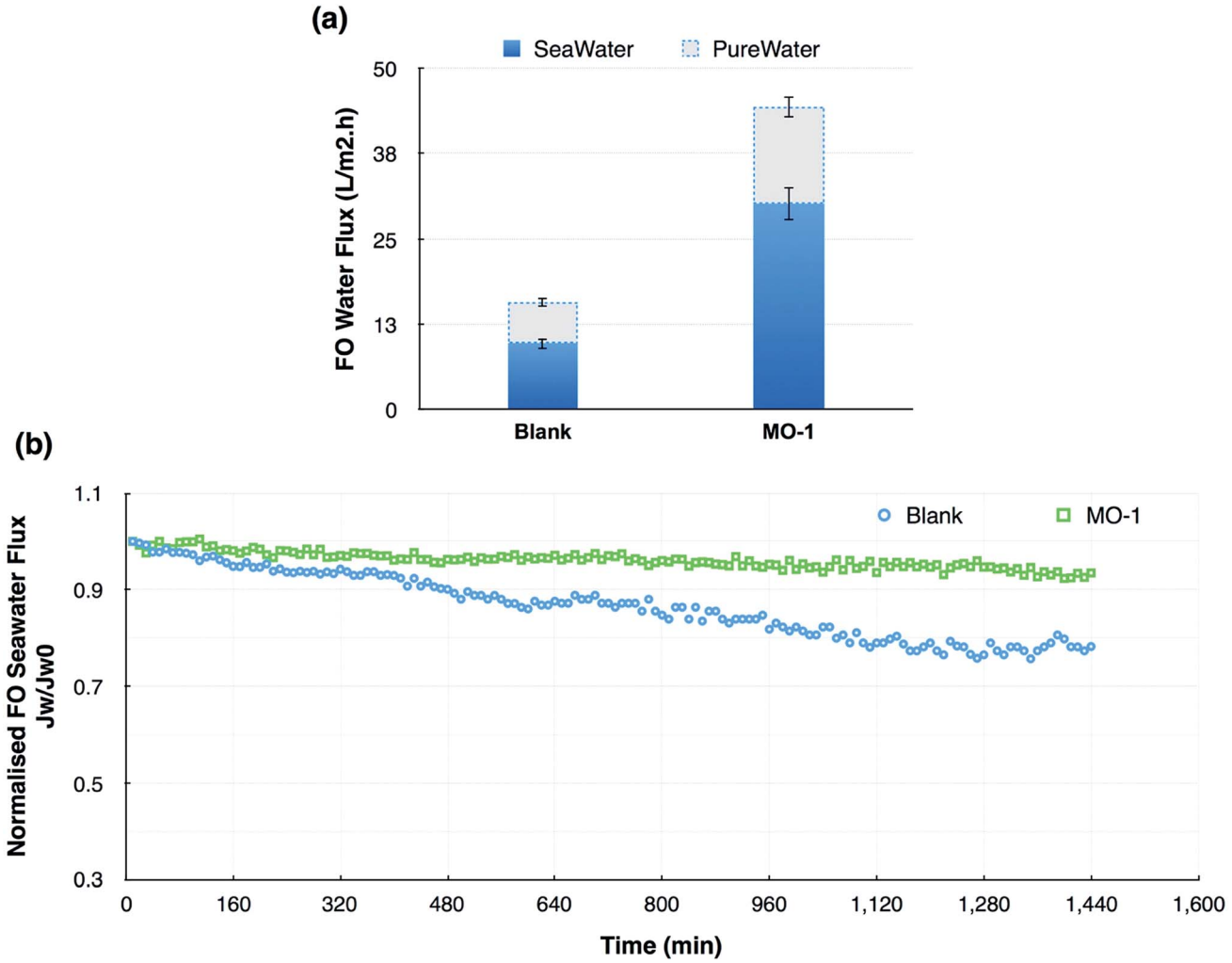

Fig. 9 A comparison between water flux of the blank and MO-1 membranes using the Caspian seawater as FS and 2 M NaCl DS in ALFS orientation, (a) comparison between pure water and seawater flux at the beginning of the experiment, (b) desalination performance stability over time ($T = 25$ °C).

Incorporating MOF into CTA matrix offers a number of advantages to reduce S parameter. The results of membrane characterization confirmed that the MO-1 membrane had superior porosity as well as hydrophilicity compared to the unmodified membrane (Table 2 and Fig. 1). The higher porosity linearly affects the membrane S parameter, whereas the hydrophilicity has an indirect influence on the S parameter. Improving the membrane hydrophilicity (wettability) can maximize as well as minimize the effective porosity and tortuosity, respectively.[29,68] These effective features refer to the membrane interconnected region, which can be saturated with water and may be available for water transport. Likewise, the pore network within the MOF particles may further enhance the continuity of water pathways and thus reduces the tortuosity value of the modified membranes. Furthermore, prominent feature of the high-surface area of MOF could enable high-water adsorption capacity.[47,69] Both the higher porosity and the lesser tortuosity resulted in a lower ratio of τ/ε in the modified membrane. These may explain why the MOF particles reduced the S parameter in the modified membranes. However, the higher S parameter in the MO-2 membrane compared to the MO-1 is attributed to a lower degree of porosity and so a higher ratio of τ/ε.

Specific salt flux (J_s/J_w) represents the amount of DS loss per unit of water produced in FO process. A lower J_s/J_w ratio is desirable as it indicates a higher selectivity as well as efficiency to avoid the DS loss and accordingly severe ICP.[67,70,71] As shown in Fig. 7, low content of MOF particles in the MO-1 membrane led to the lowest J_s/J_w ratio in all DS concentrations, indicating an excellent water transport without reducing the membrane selectivity. While the high MOF content in the MO-2 membrane caused to the highest J_s/J_w ratio, demonstrating a declined trend for its selectivity.

In the case of the MO-1 membrane, the observed decline in the specific salt flux, J_s/J_w, compared to the blank membrane is attributed to its considerably enhanced A value without decreasing in the selectivity. Whereas, the less selective layer integrity for the MO-2 membrane resulted in a higher salt

permeability, B, and thus increase in J_s/J_w ratio. The theory of FO specific salt flux can support the observed results because there are a linear relationship between the experimental value of J_s/J_w and the intrinsic membrane active layer characteristics ratio, B/A.[67] At high J_s/J_w ratio, the FO water flux decreases as the high salt concentration increases the ICP and decreases the effective osmotic pressure across the membrane. This also describes the decrease in the FO water flux through the MO-2 membrane as compared to the MO-1 membrane.

It can be concluded that a proper amount of MOF can considerably improve the membrane properties and FO performance as well. The high loading rate may lead to particle agglomeration in the membrane matrix, and consequently may have the negative effects on the membrane structure and performance.

3.3. Antifouling properties of the membranes

Fig. 8 represents the fouling curves for the blank and MO-1 membranes. The curves present the slight decline in water flux for both membranes due to fouling caused by extremely high foulant concentration (Fig. 8a). The MO-1 membrane exhibited smaller water flux decline (about 24%) than the blank membranes (around 40%). Fig. 8b shows the membranes flux recovery, demonstrating a greater recovery of water flux for the MO-1 membrane. Both results, smaller flux decline and higher flux recovery, confirm the higher antifouling property for MOF mixed matrix membrane.

The reverse diffusion of draw solute to the FS results in salts accumulated region at the active layer and feed stream interface. This phenomenon reduces the effective osmotic driving force, and hence a reduction of the FO water flux. Alginate layer that accumulate on the membrane surface exacerbate these effects through cake-enhanced osmotic pressure (CEOP).[72] Whereas the membrane surface properties can intensify or alleviate the fouling propensity.

Hydrophilic surface can provide effective alterations on the membrane surface interaction with organic foulants. The thin water film that forms on a hydrophilic surface through hydrogen bonding prevents deposition of foulants and thus provides a lower fouling propensity.[73] Therefor, the lower water flux decline of the MO-1 membrane can be attributed to its more hydrophilic surface which is the result of MOF loading. On the other hand, rougher surface can enhance fouling tendency on the membrane surface because of greater surface area for foulants attachment and possibility of their accumulation in valley.[74] The fouling experiment results obviously indicated that in this case, the surface hydrohplicity of the MO-1 membrane predominantly resulted in an advanced antifouling property for MOF mixed matrix membrane.

3.4. Seawater desalination performance

In order to verify the opportunity of MOF loading in enhancing desalination performance of the FO membranes, the blank and MO-1 membranes were examined using the Caspian seawater and 2 M NaCl solution as FS and DS, respectively. Fig. 9 shows the corresponding results. The seawater composition was presented in ESI (Table S2†). The MO-1 membrane demonstrated a noteworthy seawater flux of almost 30 L m^{-2} h^{-1} at the beginning of experiment, while the FO seawater flux through the blank membrane was approximately 10 L m^{-2} h^{-1} (Fig. 9a). Correspondingly, the membranes were continuously tested under seawater desalination, and the results of FO water flux decline during time were presented in Fig. 9b. The MO-1 membrane exhibited a very stable FO water flux during the entire testing period, so that only 6% reduction was observed that the initial flux. Instead, the blank membrane showed much more reduction in water flux (about 22%) than its initial flux. These observed FO water flux decline during seawater desalination are attributed predominantly to membrane fouling and DS dilution. As discussed in the membrane characterization,

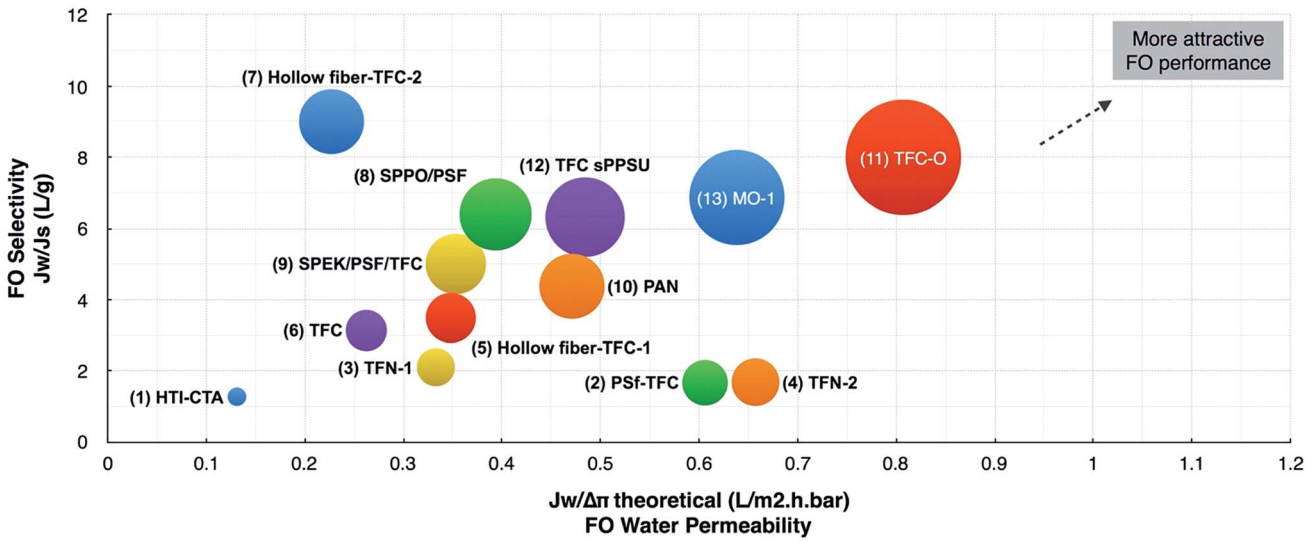

Fig. 10 Comparisons of FO performance of the MOF modified membrane with various FO membranes in literature. (Orientation = ALFS, feed = DI water, DS = NaCl 0.5–2 M, T = 20–25 °C).

MOF loading caused a higher water permeability and lower S parameter in the MO-1 membrane than those of the blank membrane. Thus, it is not surprising to see a much higher FO water flux through the MO-1 membrane during seawater desalination. Likewise, the more stable FO water flux of the MO-1 membrane during seawater desalination can be attributed to its antifouling properties which is provided by MOF loading.

3.5. Performance comparison with other FO membranes reported in literature

Fig. 10 compares the FO performance of MO-1 membrane developed in this study *versus* other FO membranes in the literature. The data were presented in ESI (Table S3†) where references were also provided. This graph presents a trade-off between FO water permeability (J_w to the theoretical osmotic pressure) and FO selectivity (J_s/J_w, specific salt flux). The high degree of perm-selectivity is essential for a high-performance FO membrane. A greater circle means superior overall performance in terms of both FO perm-selectivity. The MO-1 membrane containing 3 wt% MOF exhibited high performance of FO water permeability as well as selectivity, compared to other recent FO membranes. Moreover, the performance of MO-1 membrane is comparable with newly developed TFC membrane by R. C. Ong *et al.*[23] While, cellulose esters based membranes may be preferred because of their intrinsic advantages including low cost, wide availability, high hydrophilicity, low fouling and superior chlorine resistance.[43,44]

4. Conclusions

The MOF was successfully embedded within the CTA membrane matrix to improve the performance of FO membranes. The characterization results indicated that the MOF particles existed within the membrane matrix and improved its properties in terms of perm-selectivity and structural parameter. Hydrophilic surface and highly porous structure of Cu-BTC particles can selectively absorb water and provide alternative transport pathways for water media through the membrane. Improving the membrane hydrophilicity predominantly resulted in an advanced antifouling property for MOF mixed matrix membrane. The modified membrane exhibited much higher performance in FO process as well as desalination, compared to the most FO membranes developed in recent studies. These observations suggest that MOFs can take the FO membranes to the next level of performance and capability.

References

1 M. Obaid, Z. K. Ghouri, O. A. Fadali, K. A. Khalil, A. A. Almajid and N. A. M. Barakat, *ACS Appl. Mater. Interfaces*, 2016, **8**, 4561–4574.
2 T.-S. Chung, S. Zhang, K. Y. Wang, J. Su and M. M. Ling, *Desalination*, 2012, **287**, 78–81.
3 S. Zhao, L. Zou, C. Y. Tang and D. Mulcahy, *J. Membr. Sci.*, 2012, **396**, 1–21.
4 R. Valladares Linares, Z. Li, V. Yangali-Quintanilla, N. Ghaffour, G. Amy, T. Leiknes and J. Vrouwenvelder, *Water Res.*, 2016, **88**, 225–234.
5 W. Xie, F. He, B. Wang, T.-S. Chung, K. Jeyaseelan, A. Armugam and Y. W. Tong, *J. Mater. Chem. A*, 2013, **1**, 7592–7600.
6 Z. Jia and Y. Wang, *J. Mater. Chem. A*, 2015, **3**, 4405–4412.
7 R. Valladares Linares, Z. Li, S. Sarp, S. S. Bucs, G. Amy and J. Vrouwenvelder, *Water Res.*, 2014, **66**, 122–139.
8 T. Y. Cath, A. E. Childress and M. Elimelech, *J. Membr. Sci.*, 2006, **281**, 70–87.
9 Y. Cai, W. Shen, J. Wei, T. H. Chong, R. Wang, W. B. Krantz, A. G. Fane and X. Hu, *Environ. Sci.: Water Res. Technol.*, 2015, **1**, 341–347.
10 J. Ren and J. R. McCutcheon, *Desalination*, 2014, **343**, 187–193.
11 D. Li and H. Wang, *J. Mater. Chem. A*, 2013, **1**, 14049–14060.
12 G. Han, T.-S. Chung, M. Toriida and S. Tamai, *J. Membr. Sci.*, 2012, **423**, 543–555.
13 K. Y. Wang, T. S. Chung and G. Amy, *AIChE J.*, 2012, **58**, 770–781.
14 Q. Saren, C. Q. Qiu and C. Y. Tang, *Environ. Sci. Technol.*, 2011, **45**, 5201–5208.
15 P. Zhong, X. Fu, T.-S. Chung, M. Weber and C. Maletzko, *Environ. Sci. Technol.*, 2013, **47**, 7430–7436.
16 P. Sukitpaneenit and T.-S. Chung, *Environ. Sci. Technol.*, 2012, **46**, 7358–7365.
17 J. Wei, C. Qiu, C. Y. Tang, R. Wang and A. G. Fane, *J. Membr. Sci.*, 2011, **372**, 292–302.
18 N. Y. Yip, A. Tiraferri, W. A. Phillip, J. D. Schiffman and M. Elimelech, *Environ. Sci. Technol.*, 2010, **44**, 3812–3818.
19 S. Zhang, K. Y. Wang, T.-S. Chung, Y. Jean and H. Chen, *Chem. Eng. Sci.*, 2011, **66**, 2008–2018.
20 H. Jin, Y. Huang, H. Li, P. Yu and Y. Luo, *RSC Adv.*, 2015, **5**, 79774–79782.
21 Y. Huang, H. Jin, H. Li, P. Yu and Y. Luo, *RSC Adv.*, 2015, **5**, 106113–106121.
22 W. Ding, J. Cai, Z. Yu, Q. Wang, Z. Xu, Z. Wang and C. Gao, *J. Mater. Chem. A*, 2015, **3**, 20118–20126.
23 R. C. Ong, T.-S. Chung, J. S. de Wit and B. J. Helmer, *J. Membr. Sci.*, 2015, **473**, 63–71.
24 N. Ma, J. Wei, S. Qi, Y. Zhao, Y. Gao and C. Y. Tang, *J. Membr. Sci.*, 2013, **441**, 54–62.
25 J. Li, L. Yin, G. Qiu, X. Li, Q. Liu and J. Xie, *J. Mater. Chem. A*, 2015, **3**, 6781–6786.
26 G. D. Mehta and S. Loeb, *J. Membr. Sci.*, 1979, **4**, 261–265.
27 J. R. McCutcheon and M. Elimelech, *J. Membr. Sci.*, 2006, **284**, 237–247.
28 J.-G. Gai and X.-L. Gong, *J. Mater. Chem. A*, 2014, **2**, 425–429.
29 J. R. McCutcheon and M. Elimelech, *J. Membr. Sci.*, 2008, **318**, 458–466.
30 J.-G. Gai, X.-L. Gong, W.-W. Wang, X. Zhang and W.-L. Kang, *J. Mater. Chem. A*, 2014, **2**, 4023–4028.
31 N. Widjojo, T.-S. Chung, M. Weber, C. Maletzko and V. Warzelhan, *Chem. Eng. J.*, 2013, **220**, 15–23.
32 A. Tiraferri, N. Y. Yip, W. A. Phillip, J. D. Schiffman and M. Elimelech, *J. Membr. Sci.*, 2011, **367**, 340–352.

33 L. Shi, S. Chou, R. Wang, W. Fang, C. Tang and A. Fane, *J. Membr. Sci.*, 2011, **382**, 116–123.
34 D. Emadzadeh, W. Lau, T. Matsuura, A. Ismail and M. Rahbari-Sisakht, *J. Membr. Sci.*, 2014, **449**, 74–85.
35 N. Niksefat, M. Jahanshahi and A. Rahimpour, *Desalination*, 2014, **343**, 140–146.
36 A. Zirehpour, A. Rahimpour, F. Seyedpour and M. Jahanshahi, *Desalination*, 2015, **371**, 46–57.
37 Z. Liu, H. Yu, G. Kang, X. Jie, Y. Jin and Y. Cao, *J. Membr. Sci.*, 2016, **497**, 485–493.
38 H. B. T. Jeazet, C. Staudt and C. Janiak, *Dalton Trans.*, 2012, **41**, 14003–14027.
39 X. L. Liu, Y. S. Li, G. Q. Zhu, Y. J. Ban, L. Y. Xu and W. S. Yang, *Angew. Chem., Int. Ed.*, 2011, **50**, 10636–10639.
40 G. M. Shi, T. Yang and T. S. Chung, *J. Membr. Sci.*, 2012, **415**, 577–586.
41 S. Basu, M. Maes, A. Cano-Odena, L. Alaerts, D. E. De Vos and I. F. Vankelecom, *J. Membr. Sci.*, 2009, **344**, 190–198.
42 S. Sorribas, P. Gorgojo, C. Téllez, J. Coronas and A. G. Livingston, *J. Am. Chem. Soc.*, 2013, **135**, 15201–15208.
43 A. Sagle and B. Freeman, *The future of desalination in Texas*, 2004, vol. 2, pp. 137–154.
44 B. Mi and M. Elimelech, *J. Membr. Sci.*, 2008, **320**, 292–302.
45 P. Küsgens, M. Rose, I. Senkovska, H. Fröde, A. Henschel, S. Siegle and S. Kaskel, *Microporous Mesoporous Mater.*, 2009, **120**, 325–330.
46 X. Yan, S. Komarneni, Z. Zhang and Z. Yan, *Microporous Mesoporous Mater.*, 2014, **183**, 69–73.
47 S. Khoshhal, A. A. Ghoreyshi, M. Jahanshahi and M. Mohammadi, *RSC Adv.*, 2015, **5**, 24758–24768.
48 R. Wang, L. Shi, C. Y. Tang, S. Chou, C. Qiu and A. G. Fane, *J. Membr. Sci.*, 2010, **355**, 158–167.
49 Q. Yang, K. Y. Wang and T.-S. Chung, *Environ. Sci. Technol.*, 2009, **43**, 2800–2805.
50 A. Tiraferri, N. Y. Yip, A. P. Straub, S. R.-V. Castrillon and M. Elimelech, *J. Membr. Sci.*, 2013, **444**, 523–538.
51 X. Lu, S. Romero-Vargas Castrillón, D. L. Shaffer, J. Ma and M. Elimelech, *Environ. Sci. Technol.*, 2013, **47**, 12219–12228.
52 S. R.-V. Castrillón, X. Lu, D. L. Shaffer and M. Elimelech, *J. Membr. Sci.*, 2014, **450**, 331–339.
53 X. Lu, L. H. Arias Chavez, S. Romero-Vargas Castrillón, J. Ma and M. Elimelech, *Environ. Sci. Technol.*, 2015, **49**, 1436–1444.
54 G. R. Guillen, Y. Pan, M. Li and E. M. V. Hoek, *Ind. Eng. Chem. Res.*, 2011, **50**, 3798–3817.
55 M.-J. Han and S.-T. Nam, *J. Membr. Sci.*, 2002, **202**, 55–61.
56 K.-W. Lee, B.-K. Seo, S.-T. Nam and M.-J. Han, *Desalination*, 2003, **159**, 289–296.
57 S. Mohsenpour, A. Safekordi, M. Tavakolmoghadam, F. Rekabdar and M. Hemmati, *Polymer*, 2016, **97**, 559–568.
58 Q.-Z. Zheng, P. Wang, Y.-N. Yang and D.-J. Cui, *J. Membr. Sci.*, 2006, **286**, 7–11.
59 Z. Fan, Z. Wang, N. Sun, J. Wang and S. Wang, *J. Membr. Sci.*, 2008, **320**, 363–371.
60 D. Rana, T. Matsuura, R. Narbaitz and C. Feng, *J. Membr. Sci.*, 2005, **249**, 103–112.
61 M. Norddin, A. Ismail, D. Rana, T. Matsuura and S. Tabe, *J. Membr. Sci.*, 2009, **328**, 148–155.
62 C. Y. Tang, Q. She, W. C. Lay, R. Wang and A. G. Fane, *J. Membr. Sci.*, 2010, **354**, 123–133.
63 K. Y. Wang, R. C. Ong and T.-S. Chung, *Ind. Eng. Chem. Res.*, 2010, **49**, 4824–4831.
64 S. Zhang, K. Y. Wang, T.-S. Chung, H. Chen, Y. Jean and G. Amy, *J. Membr. Sci.*, 2010, **360**, 522–535.
65 M. Moaddeb and W. J. Koros, *J. Membr. Sci.*, 1997, **125**, 143–163.
66 S. Zou, Y. Gu, D. Xiao and C. Y. Tang, *J. Membr. Sci.*, 2011, **366**, 356–362.
67 W. A. Phillip, J. S. Yong and M. Elimelech, *Environ. Sci. Technol.*, 2010, **44**, 5170–5176.
68 N.-N. Bui and J. R. McCutcheon, *Environ. Sci. Technol.*, 2013, **47**, 1761–1769.
69 J. M. Castillo, T. J. Vlugt and S. Calero, *J. Phys. Chem. C*, 2008, **112**, 15934–15939.
70 N. T. Hancock and T. Y. Cath, *Environ. Sci. Technol.*, 2009, **43**, 6769–6775.
71 Q. She, X. Jin and C. Y. Tang, *J. Membr. Sci.*, 2012, **401**, 262–273.
72 S. Lee, C. Boo, M. Elimelech and S. Hong, *J. Membr. Sci.*, 2010, **365**, 34–39.
73 C. Van Oss, W. Wu, A. Docoslis and R. Giese, *Colloids Surf., B*, 2001, **20**, 87–91.
74 E. M. Vrijenhoek, S. Hong and M. Elimelech, *J. Membr. Sci.*, 2001, **188**, 115–128.